Plasma Sci. Technol. **26** (2024) 095103 (15pp) https://doi.org/10.1088/2058-6272/ad56ca

Simulation of charge-exchange induced NBI losses on EAST

Zhanhong LIN (林展宏)[1], **Feng WANG** (王丰)[1,*], **Ming XU** (徐明)[2], **Chaofeng SANG** (桑超峰)[1], **Chen ZHANG** (张晨)[1] and **Zhengxiong WANG** (王正汹)[1,*]

[1] Key Laboratory of Materials Modification by Beams of the Ministry of Education, School of Physics, Dalian University of Technology, Dalian 116024, People's Republic of China
[2] Institute of Plasma Physics, Chinese Academy of Sciences, Hefei 230031, People's Republic of China

[*]E-mail of corresponding authors: zxwang@dlut.edu.cn and fengwang@dlut.edu.cn

Received 9 November 2023, revised 7 June 2024
Accepted for publication 11 June 2024
Published 5 August 2024

Abstract

The neutral beam injection is widely adopted in tokamaks as a key heating tool, playing a crucial role in generating burning plasmas. However, the loss of beam ions can damage the first wall and reduce the heating efficiency, resulting in failure to maintain steady-state conditions. In this work, the effect of neutral particles in the edge on fast ions generated by NBI in the Experimental Advanced Superconducting Tokamak (EAST) device is studied using the particle tracer code (PTC). The poloidal distribution of neutral particles is calculated by edge plasma simulation code SOLPS-ITER. In this simulation, four beam lines in EAST are considered: co-current tangential (co-tang), co-current perpendicular (co-perp), counter-current tangential (ctr-tang) and counter-current perpendicular (ctr-perp). It is shown that, in the absence of neutral particles, the loss fraction of ctr-injection is considerably higher than that of the co-injection. When considering the neutral particles, it is found that the ctr-perp injection demonstrates a significant variation in particles loss fraction (ranging from 18.56% to 25.42%) compared to the other three injection configurations. In terms of the loss fraction induced by neutral particles, ctr-injection exceeds co-injection, and perpendicular configuration exceeds tangential configuration. Furthermore, the difference of charge exchange ratios of three different energy (full energy, half energy, one third energy) of the four injections can be attributed to variations in the poloidal trajectories associated with each of these injections. Moreover, approximately half of fast ions which undergo neutralization directly lose to the first wall while the rest re-enter the bulk plasma and re-ionize. Except for the ctr-tang injection, the reionization ions from the other three injections exhibit effective confinement.

Keywords: NBI, charge exchange, fast ion loss

(Some figures may appear in colour only in the online journal)

1. Introduction

Neutral beam injection (NBI) is one of the most efficient auxiliary heating methods [1–3] in fusion reactor, such as TFTR [4, 5]and JET [6]. Its heating mechanism is independent of any resonance or coupling conditions and remains insensitive to plasma variations. In deuterium-tritium (D-T) fusion reaction, NBI plays a key role in achieving high D-T fusion performance, with 11.9 MW D-NB and 10.5 MW T-NB in JET discharge and 14.2 MW D-NB and 25.3 MW T-NB in TFTR discharge [7]. To meet the requirement of fusion energy of burning plasma, it is necessary to investigate heating efficiency and confinement of fast ions of NBI [8].

The Experimental Advanced Superconducting Tokamak (EAST) is equipped with two sets of deuterium beam injec-

* Authors to whom any correspondence should be addressed.

tion systems: a co-current system and a counter-current system [9]. These installations are of significant importance in realizing long-pulse (1000 s), high-performance and advanced steady-state operations. The confinement of energetic particles originating from NBI is an important issue in EAST device. The lost fast ions can generate substantial localized heat loads on the wall, resulting in damage to the plasma-facing components and potentially even triggering plasma extinguishment [10–14]. In recent years, some numerical investigations have been conducted on various aspects of NBI on EAST device, including first-orbit losses of NBI [13], NBI fast ion loss in the presence of toroidal field ripple [14], effect of resonant magnetic perturbations on NBI [15] and the effect of NBI on the excitation and suppression of fast ion instabilities as well as the resultant losses [16]. In previous simulations, the influence of neutral particles from the scrape-off layer (SOL) on the confinement of beam ions was often neglected. The SOL is located between the last closed flux surface (LCFS) and the first wall, usually containing a substantial population of neutral particles [17, 18]. During the process of NBI, some fast ions are deposited at the edge (near the LCFS), and owing to drift effects, a part of the fast ions also traverse LCFS. Fast ions near the SOL can undergo charge exchange reactions with neutral particles, leading to their conversion into fast neutrals. Subsequently, these fast neutrals may either be lost by impacting the first wall, or re-enter the bulk plasma where they will undergo re-ionization processes. This phenomenon was observed by fast-ion D-alpha (FIDA) spectroscopy system in NBI experiment conducted on the TCV tokamak [19]. The neutral particles originating from the SOL can lead to an increased heat load on the first wall. Therefore, it is crucial to understand the effect of these neutral particles from the SOL clearly.

Some pioneering works on the effect of neutral particles from the SOL on beam ions have been conducted in recent years. For example, in the works of Kramer *et al* [20] and Jaulmes *et al* [21], the interaction between neutral particles and beam ions on DIII-D tokamak and COMPASS upgrade tokamak has been studied. However, a constant neutral density in the SOL was used in their simulations since the experimental determination of neutral density in SOL remains limited. In fact, the density of neutral particle near the divertor region is notably greater than that in the midplane, so the neutral particle distribution is substantially different in poloidal direction. Hence, to precisely simulate the effect of charge exchange on fast ion losses on EAST device, it is necessary to take the realistic distribution of neutral particles in poloidal direction into consideration.

In this article, the distribution of neutral particles in the SOL is provided by SOLPS-ITER simulation [22, 23], which calculates their distribution at a normalized radius of $\rho \sim 0.8$–1.1. Additionally, beam ion deposition, fast ion motion in magnetic fields and charge exchange processes are calculated by particle tracer code (PTC) [24]. Some meaningful works have been carried out by PTC [25, 26]. The NBI module has been integrated into the newest version of PTC, and the benchmark with NUBEAM [27] and NEMO [28] has been done yet. The effect of neutral particles from SOL on beam ions from co-injection and ctr-injection on EAST device is numerically studied in this work. Four beam lines in EAST are considered, it is found that ctr-perp injection exhibits a significant variation in particle loss fraction. Furthermore, the ratios of charge exchange of three different energy of four injections are different. Besides, reionization leads to a reduction of roughly 50% in the fraction of lost neutral particles of four injections. The article is organized as follows. Section 2 describes basic physical parameters and simulation setup. Section 3 shows the results, including the losses without neutrals, losses with neutrals and losses with neutrals and reionization. Finally, summary and discussion are presented in section 4.

2. Basic physical parameters and simulation setup

2.1. Plasma equilibrium and NBI configuration

EAST is a superconducting tokamak with major radius $R_0 = 1.85$ m, minor radius $a \approx 0.45$ m [29, 30]. Figure 1 gives the equilibrium profiles with normalized poloidal magnetic flux $\psi_{\rm p}$, and magnetic configuration is shown in figure 2. The profile of electron density is provided by polarimeter interferometer (POINT) system [45], the profile of electron temperature is measured by Thomson scattering (TS) diagnostic [46], the profile of ion temperature is measured by the Charge eXchange Recombination Spectroscopy (CXRS) [47]. The Θ describes the poloidal position of the wall and the definition of Θ in figure 2 is the length from right side of limiter to any point of limiter divides by perimeter of limiter, the direction is anticlockwise. The equilibrium profiles were reconstructed by EFIT code from EAST discharge #51063 @4.0 s, and the constraints derived from experimental diagnostics are considered in reconstruction process. The NBI systems installed in the EAST contain both co-current injection and counter-current injection configurations (recently the counter-current injection was replaced by another co-current injection in upgraded NBI system). Each individual beam injec-

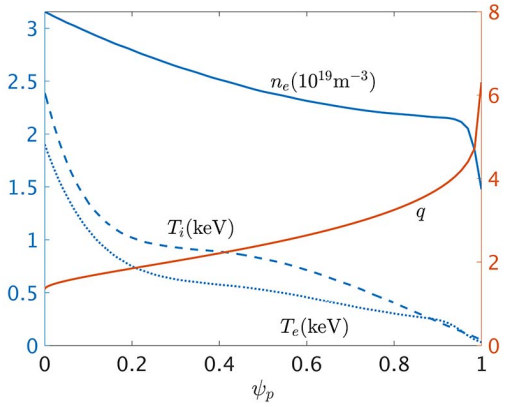

Figure 1. The profiles of ion temperature $T_{\rm i}$, electron temperature $T_{\rm e}$, electron density $n_{\rm e}$ and safety factor q on EAST discharge #51063 @4.0 s.

tor is comprised of two ion sources and each of these sources is capable of generating beam power ranging from 2 to 4 MW with an energy of 50–80 keV. The co-injection, consisting of co-tang injection and co-perp injection, is located at the A-port, and the ctr-injection, including ctr-tang injection and ctr-perp injection, is situated at the F-port, as shown in figure 3. The neutral beams are usually injected in the same toroidal direction as the plasma current in a tokamak because it can drive additional plasma current and the first-orbit losses is relatively lower. As for ctr-injection, it can be used to access the quiescent H mode of high confinement [43], besides, the toroidal angular momentum delivered to the plasma can be larger with ctr-injection [44]. In EAST experiments, it is shown that the ctr-injection can effectively heat the plasma, generate counter rotation and drive counter non-induced current, accessing the H mode of high confinement. This design facilitates the balanced injection of two beamlines, providing the NBI system in EAST with the flexibility to meet the demands of various physical studies, including counter-current NBI current drive and other related studies. The main parameters of NBI system are given in table 1 [9], the tangency radius is defined as the distance between the beamline and the center of the tokamak.

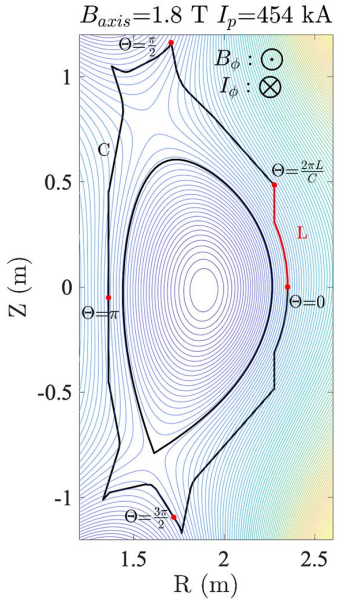

Figure 2. The magnetic configuration with B_{axis} = 1.8 T, I_p = 454 kA, plasma current is anticlockwise and toroidal magnetic field is clockwise.

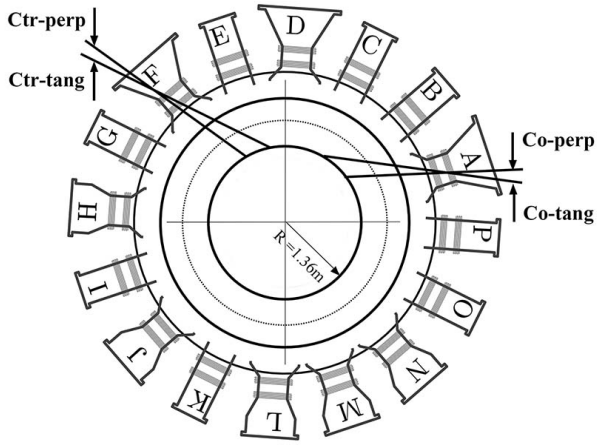

Figure 3. Top view of the NBI system of EAST. Four NBI beam lines, named co-tang, co-perp, ctr-tang, ctr-perp, are installed in A-port and F-port, and the tangency radii are 1.264 m, 0.731 m, 1.141 m, 0.606 m, respectively.

2.2. Charge exchange model

Figure 4 depicts the charge exchange process between fast ions and neutral atoms in this study, where the fast ions are the deuterium ions originating from NBI. Accurately obtaining the distribution of neutral particles at the plasma edge experimentally is challenging, hence, the neutral particles profiles employed in this work are derived from the edge plasma simulation code SOLPS-ITER and the neutral particles are mainly from divertor, as shown in figures 5 and figure 6. In addition to atomic and molecular deuterium, other neutral particle specie, such as carbon, also exists [23]. Nevertheless, in this equilibrium, the densities of other neutral particle species are several orders of magnitude lower than that of atomic deuterium. Consequently, our study only focuses on atomic and molecular deuterium. The primary charge exchange processes in this study are:

$$D^+ + D \rightarrow D + D^+ \tag{1}$$

$$D^+ + D_2 \rightarrow D + D_2^+ \tag{2}$$

the reionization process is:

$$D + D^+ \rightarrow D^+ + D^+ + e^- \tag{3}$$

Table 1. Parameters of EAST NBI system

Parameters	Design specifications
Height and width of source	120 × 480 mm^2
Beam horizontal divergence	0.6°
Beam vertical divergence	1.2°
Beam horizontal focal length	Infinite
Beam vertical focal length	10.0 m
Tangency radius of co-tang	1.264 m
Tangency radius of co-perp	0.731 m
Tangency radius of ctr-tang	1.141 m
Tangency radius of ctr-perp	0.606 m

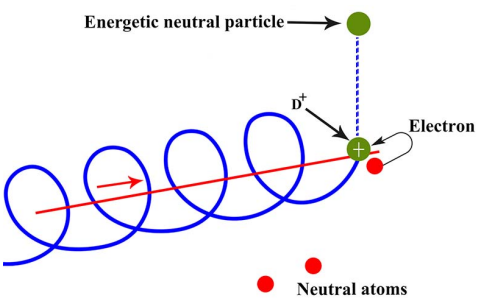

Figure 4. Charge exchange process between fast ions and neutral atoms.

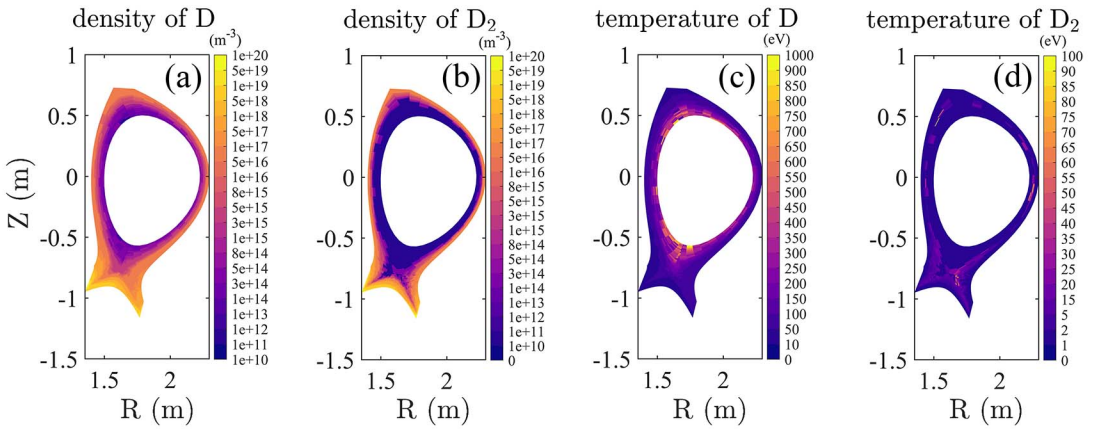

Figure 5. Poloidal distributions of (a) D atomic density n_{D}, (b) D_2 molecular density n_{D_2}, (c) D atomic temperature and (d) D_2 molecular temperature.

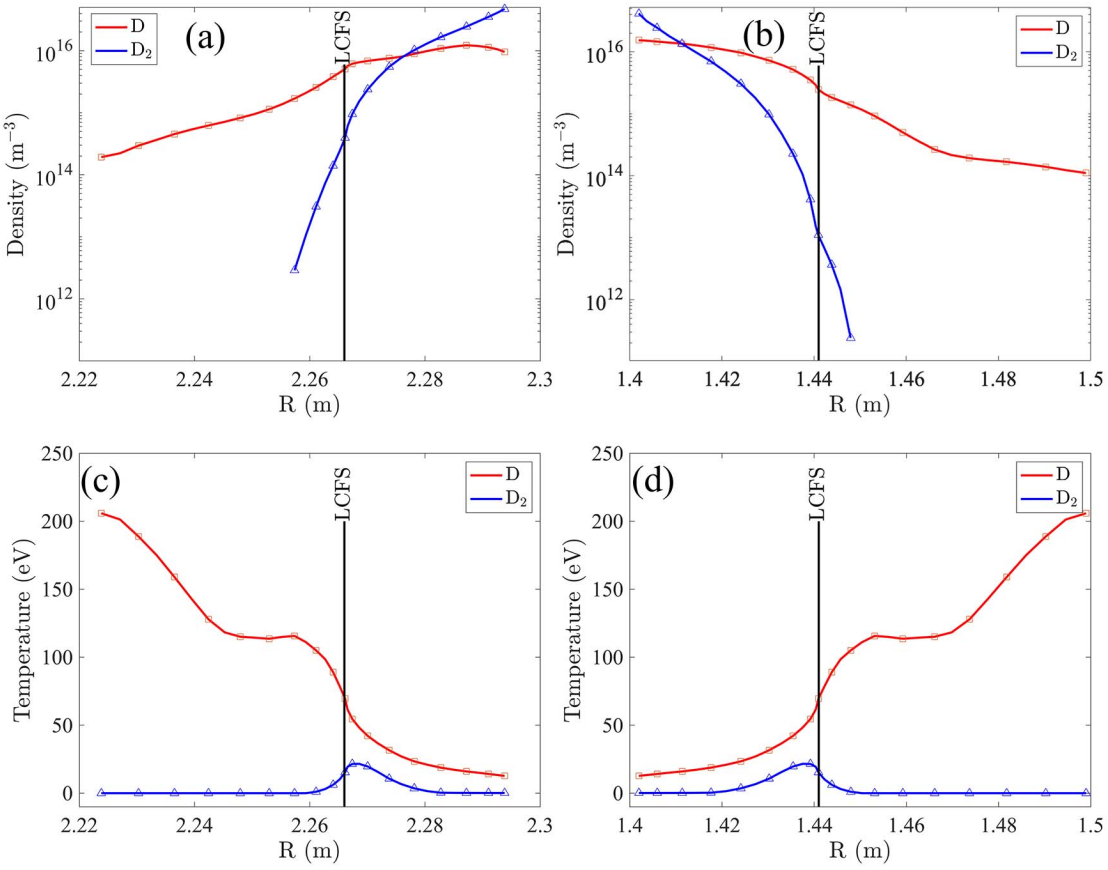

Figure 6. Distributions of density and temperature of atomic D and D_2 at outer midplane. The density and temperature in low field side are plotted in (a) and (c), respectively. The density and temperature in high field side are plotted in (b) and (d), respectively.

the probability $P(\mathrm{t})$ of an occurrence of charge exchange (or reionization) process is given as:

$$P(\mathrm{t}) = 1 - \prod\nolimits_j \exp\left(-\frac{\delta t}{\tau_{\mathrm{cx}_j}}\right), \tag{4}$$

$$\tau_{\mathrm{cx}_j} = \frac{1}{< \sigma_{N_j} v > n_{0_j}}, \tag{5}$$

with the local neutral (ion) density n_{0_j}, the time interval δt, the rate coefficient $< \sigma_{N_j} v >$ obtained from the analytic fits, σ_{N_j} is the cross section between fast ions and neutral particles, v is the collision velocity. A random number between 0 and 1 is generated during each time interval, and this number is then compared with the probability of charge exchange (or reionization) to determine whether the charge exchange (or reionization) process occurs.

2.3. Description of PTC and simulation setup

The deposition of beam ions from NBI and the process of charge exchange (or reionization) are calculated by PTC. As

a test particle program, PTC employs both guiding-center and full-orbit equations to push particles. Through conversion of phase space coordinates, a hybrid calculation of these two types of orbits is realized. With unstructured triangular meshes, the tokamak geometry, including both the core plasma and SOL region, is accurately described by PTC. When integrated with practical experimental setups, PTC provides an accurate and comprehensive depiction of fast particle transport and loss and the Monte Carlo method is used for coulomb collisions. Furthermore, the benchmark has been accomplished between PTC [24] and ORBIT [31, 32].

For the provided plasma profiles and neutral beam parameters, PTC utilizes narrow-beam model [33] to calculate the phase-space distribution of beam ions. Compared to Monte Carlo model, which requires more computational resources but provides better physical accuracy, the narrow-beam model achieves a middle ground in terms of accuracy of physical processes and computational efficiency [28]. In our simulation, the injected power of each beam line is 1 MW, the default beam energy is 51 keV and the number ratios of full, half, one third energy particles are 0.8:0.14:0.06. The ionization of the neutral beam comprises three atomic processes: charge exchange, ion-induced ionization, and electron-induced ionization. The cross sections for these processes are calculated utilizing the data from Janev [34, 35]. Figure 7(a) illustrates the initial poloidal distribution of beam ions of co-tang injection after toroidal integration, the poloidal distributions of other three injections are similar, and the top view of initial distribution of four injections are shown in figures 7(b)–(e). The fast ions in this simulation contain D^+, D_2^+, D_3^+. The shine through fraction of EAST NBI is shown in table 2. It is evident that, owing to the plasma profile's relatively low density, the shine through fraction of each beam would be high.

The gyro radius of deuterium ion at 51 keV is approximately 2 cm, because of the substantial neutral particle density and temperature gradients near the LCFS, the full orbit is required for precise charge exchange simulation. Moreover, to accurately simulate the direction of neutral particles after charge exchange, the utilization of the full orbit is a necessity. In the simulation, the time travel δt is set to ensure that each gyration period comprises 60–80 steps, thereby guaranteeing the accuracy of the simulation. We select 100000 particles from the initial distribution of beam ions as test particles, including 80000 particles with full energy, 14000 particles with half energy, and 6000 particles with one third energy. Figure 8 displays the rate coefficients of the charge exchange process for three different energy particles at a plasma temperature of 400 eV. Employing the equation (5) and adopting $n_D = 5\times10^{15}$ m^{-3} as a typical density, the estimated value for τ_{cx_D} is approximately 6 ms for full energy particles. Therefore, the simulation will take approximately 6 ms, without the consideration of slowing down, and the toroidal field ripple (TFR) has not been considered in this simulation.

3. Results

3.1. Losses without neutrals

The simulation of fast ions losses in the absence of neutral particles can provide a fundamental understanding of the effect of charge exchange. In this section, we give the results about the fraction, spatial distribution and typical trajectory

Table 2. Shine through fraction of EAST NBI in shot #51063.

Neutral beam injector	Shine through fraction (%)
Co-tang	7.66
Co-perp	14.5
Ctr-tang	10.1
Ctr-perp	15.2

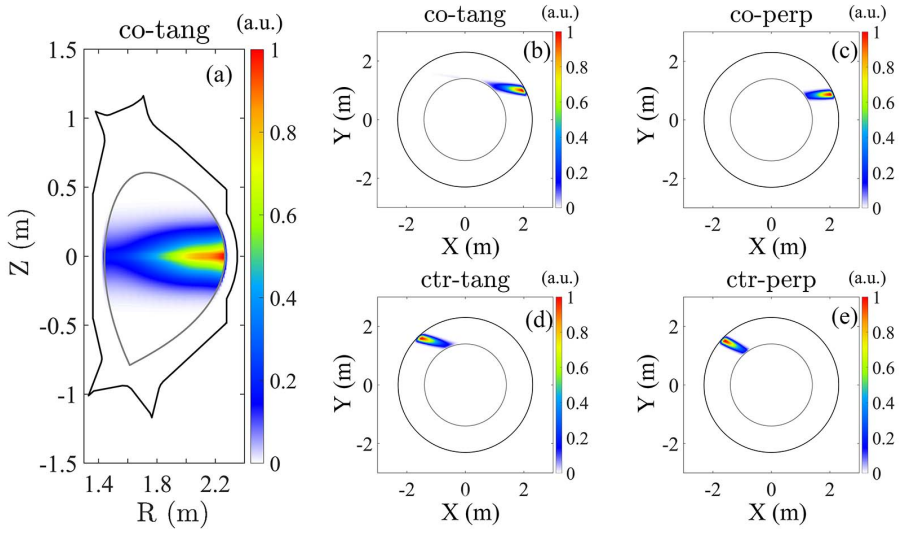

Figure 7. (a) The initial poloidal distribution of co-tang injection, (b)–(e) the top view of initial distributions of four injections, the units of colour bar are arbitrary units, the colour gradient from red to blue signifies variations in the density of fast ions, ranging from higher to lower density.

of lost particles of four injections.

Figure 9 shows the loss fraction of fast ions of four injections. Evidently, the loss fraction of ctr-injection is considerably higher than that of the co-injection. Regarding co-injection, the fast ions are well confined, the perpendicular configuration exhibits a slightly higher loss fraction compared to the tangential configuration. Considering ctr-injection, however, the confinement of fast ions is not as good as co-injection. Moreover, in ctr-injection, a significantly smaller loss fraction in the perpendicular configuration is found compared to the tangential configuration, which is the opposite of co-injection. The results of fast ions losses in the absence of neutral particles calculated by PTC are compared to the results in reference [13], which shows the validity of the PTC.

Figure 10 shows the poloidal distributions of lost power density of four injections. The definition of Θ is shown in figure 2. The lost ions from the four injections are predominantly concentrated in the region of $\Theta = \pi$–2π, corresponding to the lower hemisphere of the first wall. The peak value of the lost power density of the ctr-injection, approximately 60 kW/m^2, significantly exceeds that of the co-injection, about 10 kW/m^2.

Figure 11 plots the normalized magnetic moment of fast ions as a function of normalized canonical toroidal angular momentum. The black solid line and the red dotted line are the lost confined boundary and the trapped passing boundary, respectively. The fast ions in the region bounded by the two solid black lines are lost, and those within the region bounded by the red dashed line are trapped. The validation of the loss fractions of four injections is confirmed by the distribution of fast ions in (Λ, P_n) plane. Moreover, for co-injection, the trapped particles are well confined. However, with regard to ctr-injection, the majority of the trapped particles with a perpendicular configuration are effectively confined, whereas a substantial portion of trapped particles with tangential configuration experience loss.

Initial poloidal distribution of lost ions and the lost positions on the first wall are shown in figure 12. The red line indicates the lost positions on the first wall. Due to the low plasma density, a certain number of fast ions can deposit in high field side, as shown in figure 7. That can lead to prompt ion losses. For co-injection, the initial positions of lost fast ions are mainly situated on the high field side. Conversely, for ctr-injection, the initial positions of lost fast ions are primarily located on the low field side. Regarding the lost positions on the divertor, the fast ions of co-injection predominantly deposit on lower left divertor while the fast ions of ctr-injection primarily deposit on the lower right divertor. However, a significant proportion of fast ions are lost on the right-hand side of the first wall, whether it is co-injection or ctr-injection.

In clockwise toroidal magnetic field, the toroidal velocity directions of fast ions from co-injection are opposite to the toroidal magnetic field, if depositing in high field side, they will drift outwards and some of them may lose to the wall, like the red and blue trajectories in figure 13(a). As a comparison, we have added the trajectories of confined particles in figure 13, which are plotted in orange. The orange trajectory in figure 13(a) shows a fast ion from co-injection with an initial position in the low field side, under the effect of gradient and curvature of the magnetic field, it will drift inwards. Hence, for the fast ions from co-injection whose initial position are in the low field side, they will hardly lose to the wall. As for fast ions from ctr-injection, the toroidal velocity directions are in the same direction as the toroidal

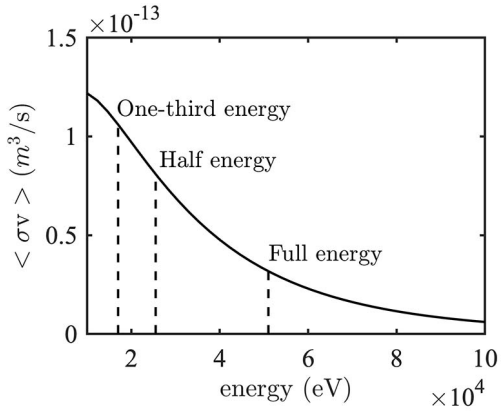

Figure 8. The rate coefficients of the charge exchange process for three different energy particles at a plasma temperature of 400 eV, data is from Janev [34, 35].

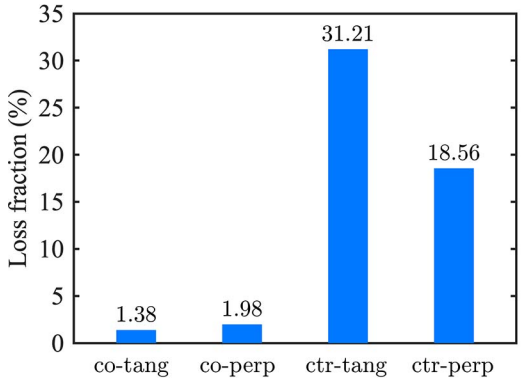

Figure 9. Fast ions' loss fractions of four injections without the influence of neutrals.

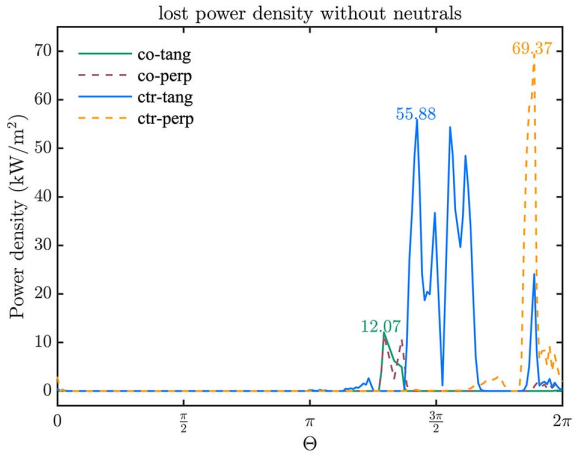

Figure 10. Lost power densities of four injections without the influence of neutrals.

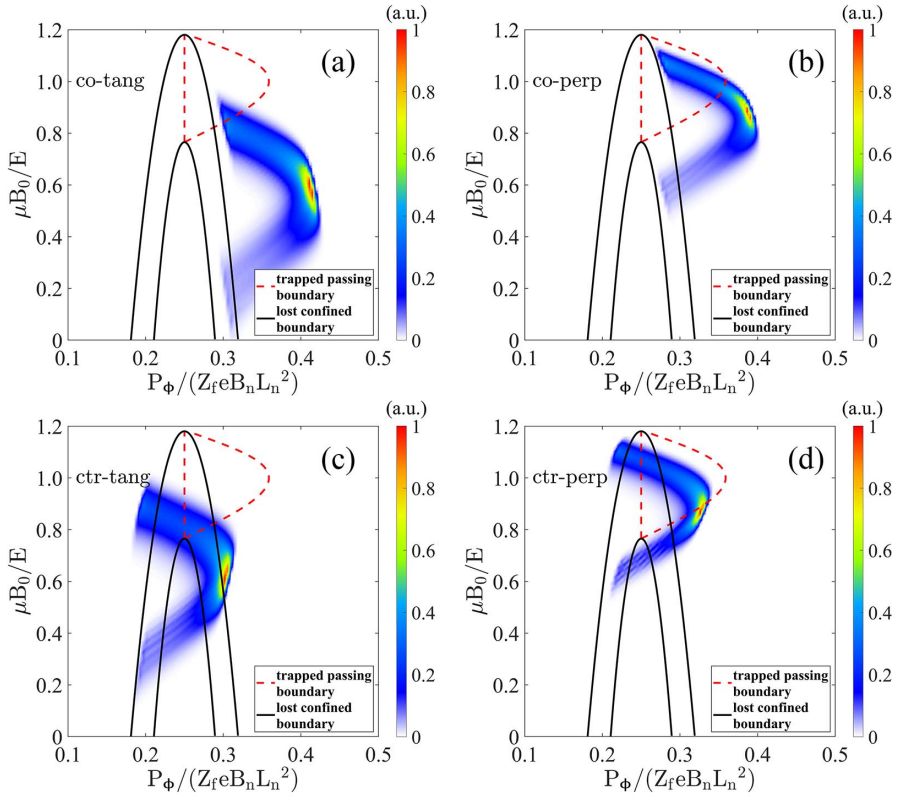

Figure 11. Distributions of fast ions in (Λ, P_n) plane of (a)–(d) four injections, where $\Lambda = \mu B_0/E$ denotes magnetic moment μ normalized by E/B_0, $P_\phi = m_f g v_\parallel/B + Z_f e\Psi$ is the canonical toroidal angular momentum and $P_n = P_\phi/Z_f e B_n L_n^2$ is the canonical toroidal angular momentum normalized by $Z_f e B_n L_n^2$. Here, B_0 is the magnetic field of magnetic axis, m_f and $Z_f e$ are the mass and charge of fast ions, Ψ is the poloidal magnetic flux function, $g = B_\phi R$, $B_n = 1$ T, $L_n = 1$ m.

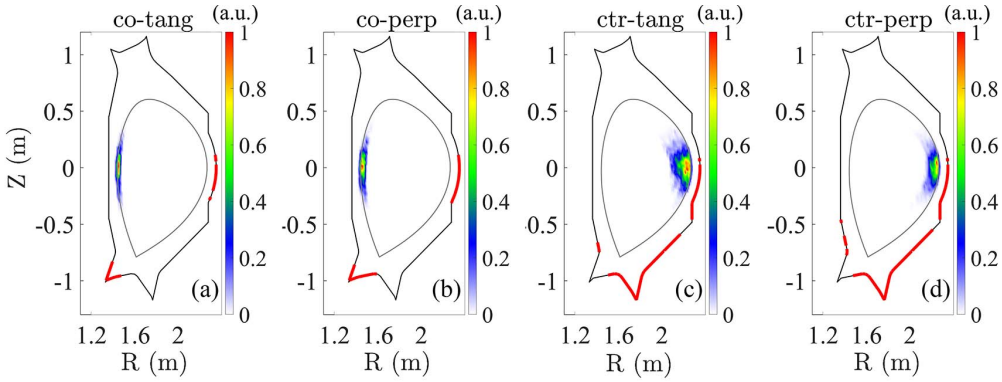

Figure 12. Initial poloidal distributions of lost fast ions and the lost positions on the first wall of (a)–(d) four injections.

magnetic field. The fast ions from ctr-injection will drift outwards if their initial positions are in the low field side, as the red, blue and purple trajectories shown in figure 13(b). In contrary, the fast ions from ctr-injection whose initial positions are in the high field side will drift inwards, as the orange trajectory in figure 13(b). Therefore, for ctr-injection, the initial positions of lost fast ions are primarily located on the low field side. The perpendicular and tangential configurations will not change the drift direction (inwards or outwards). Subsequently, for co-injection, the initial positions of lost fast ions are mainly situated on the high field side, no matter perpendicular or tangential configurations, and the initial positions of lost fast ions from ctr-tang and ctr-perp are primarily located on the low field side.

3.2. Losses with neutrals

The influence of neutral particles in the edge is discussed in this section. Density and temperature profiles of neutral particles are shown in figure 5. Figure 14 plots poloidal distribution of charge exchange particles. For co-injection, charge exchange occurs predominantly on the low field side region around the LCFS and in the lower-left divertor region. The density of charge exchange particles of co-perp injection slightly exceeds that of co-tang injection, this difference can be attributed to the increased population of trapped particles in the perpendicular configuration compared to the tangential configuration. The enhanced occurrence of charge exchange in trapped particles can be explained by their most poloidal trajectories within the

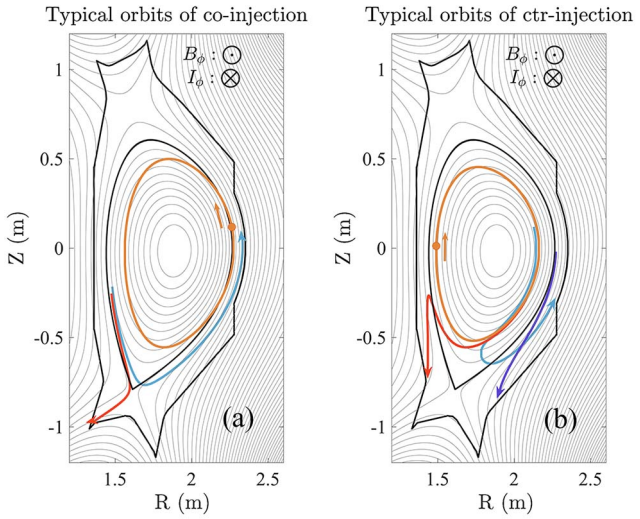

Figure 13. Typical trajectories of (a) co-injection and (b) ctr-injection. The points in orange trajectories are the initial positions of fast ions.

neutral-rich region. In contrast, only half of the poloidal trajectory of the passing particles lies within the neutral-rich region, as shown from a comparation between figures 15(a) and (b). For ctr-tang injection, charge exchange mainly occurs at lower divertor, which is different from co-injection. For ctr-perp injection, the majority of charge exchange processes occurs on the low field side region around the LCFS, with a minor occurrence on the high field side region around the LCFS, and it is noteworthy that no instance of charge exchange is observed near the lower divertor region. Figure 16 illustrates the distributions of number of charge exchange particles of three different energies as function of major radius. With the exception of ctr-tang injection, the peak value of the number of charge exchange particles at low field side (around R = 2.25 m) is observed for the remaining three injections, whereas the peak value of ctr-tang injection is found at R = 1.55 m.

Figure 17 depicts the ratios of charge exchange particles of four injections. Considering co-tang injection, the charge exchange ratio is the highest for one-third energy particles at 2.95%, followed by half energy particles at 2.35%, but the difference in charge exchange ratios between the three different energies is relatively moderate. The difference can be explained by the lower penetration of lower energies on the LCFS. The reason for this phenomenon is explicated in the figure 15(a), for co-tang injection, most of fast ions are passing particles, for particles of various energies, the differences in the segments of poloidal trajectories within the neutral-rich region are relatively small, thereby explaining the slight difference in the charge exchange ratios. Regarding co-perp injection, the charge exchange ratio for particles with full energy shows negligible variation compared to that of co-tang injection, however, the charge exchange ratios for particles with half energy and with one third energy are twice as high as those of co-tang injection. In figure 15(b), particles with one third energy remain entirely within the neutral-rich region along their poloidal trajectories, the left-side poloidal trajectory of particles with half energy closely approaches the neutral-rich region, and taking the Larmor radius into account, there is a considerable probability of charge exchange occurring along the left-side poloidal trajectory as well. Nevertheless, the left-side poloidal trajectory of particles with full energy remains distant from the neutral-rich region, resulting in a lower charge exchange ratio for particles with full energy compared to particles with half and one third energy. As for ctr-tang injection, the charge exchange ratio for particles with full energy is significantly lower compared to the other two energy particles, which can be explained by figure 15(c). A considerable fraction of full energy particles deposited near the LCFS are lost due to curvature and gradient drift effects, and the trajectories of confined full energy particles are in the region lack of neutral particle, thereby the charge exchange process of particles with full energy mainly arises from ions that are about to lose but have not experienced it yet. It is noteworthy, as shown in figure 16(c), that the number of full energy particles undergoing charge exchange is lower than the number of other two energy particles at the position where R > 1.7 m, despite accounting for 80% of the total particle population.

When neutral particles near the edge are introduced, fast ions can undergo charge exchange reactions with them. Consequently, these ions are transformed into fast neutrals. Without the control of magnetic field, these fast neutrals can be lost directly to the first wall or penetrate into the bulk plasma where subsequent reionization takes place. In this

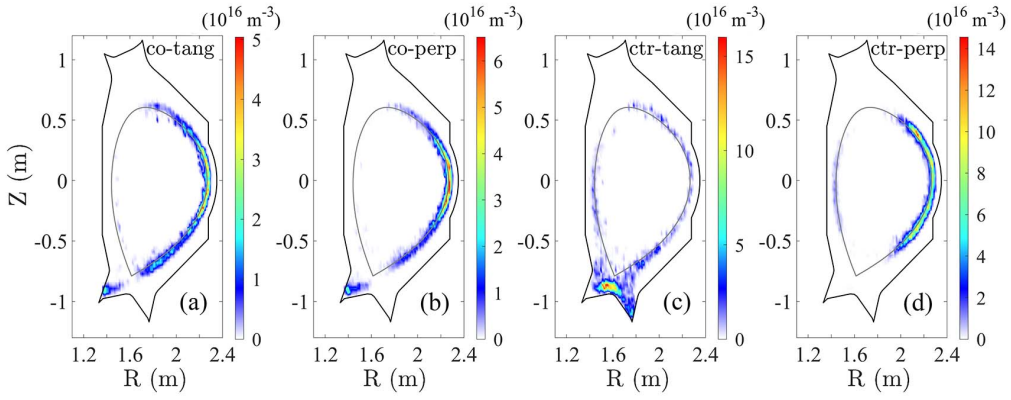

Figure 14. Poloidal distributions of density of charge exchange particles of (a)–(d) four injections.

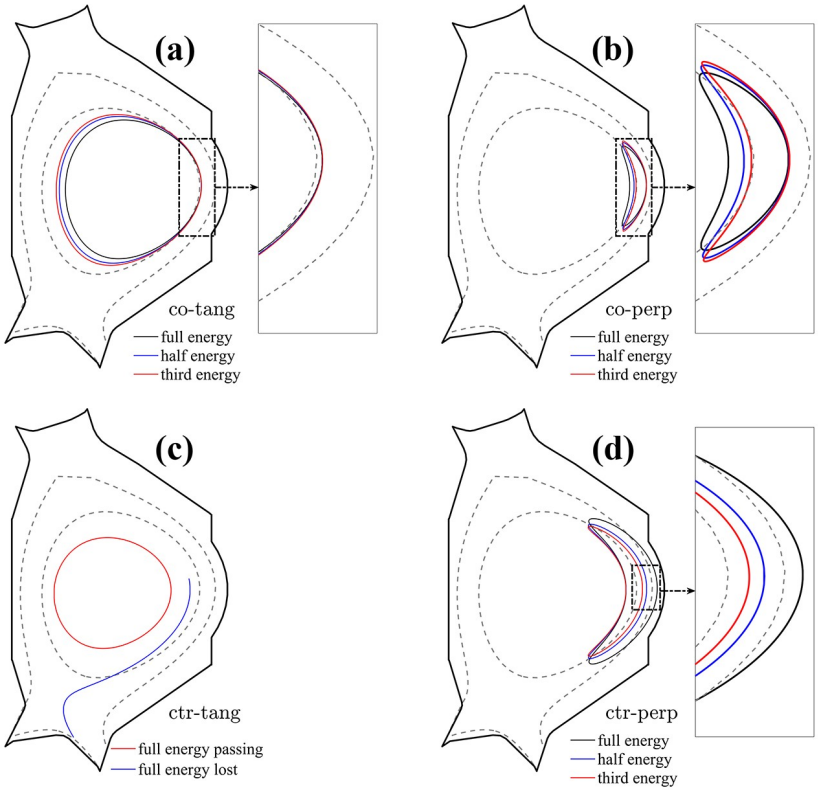

Figure 15. Typical guiding center orbit of three different energies for (a) co-tang, (b) co-perp, (c) ctr-tang, (d) ctr-perp injection. The grey-dash lines bound the region of neutral particles.

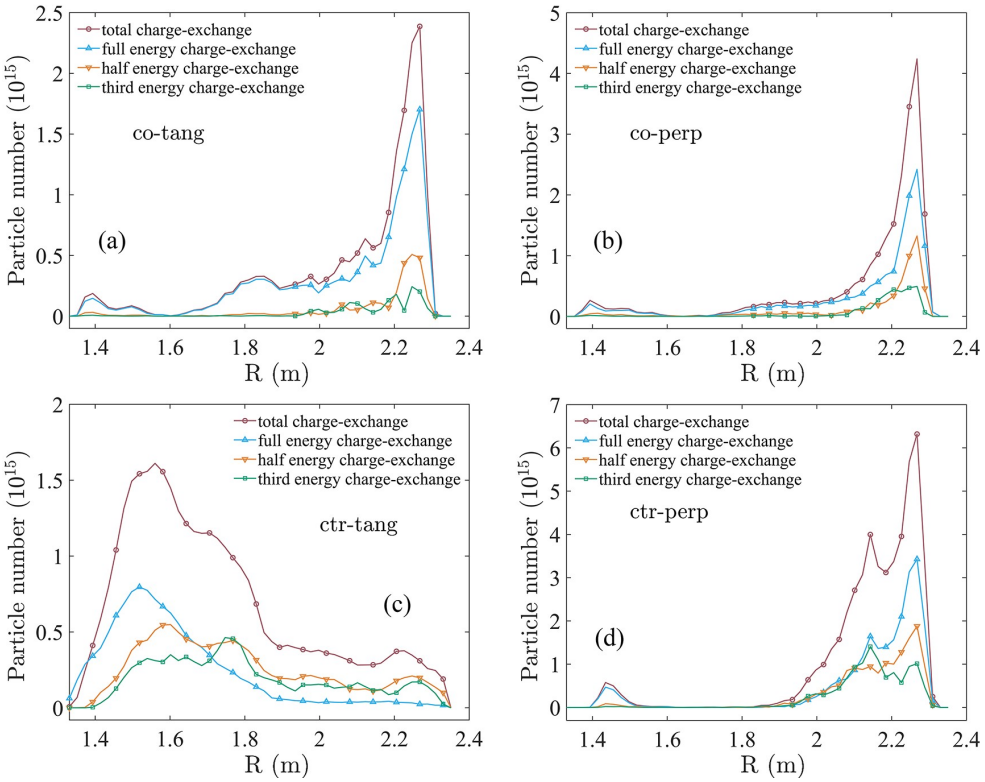

Figure 16. Distributions of charge exchange particles number of (a)–(d) four injections. It should be noted that the injected lower energy particles are less than higher energy particles and the ratios of charge exchange are plotted in figure 17.

section we focus on the effect of fast neutrals on the first wall, leaving aside the effect of reionization which will be studied in the next section.

Figure 18 plots the normalized magnetic moment of charge exchange particles as a function of normalized canonical toroidal angular momentum. The validation of the loss

fractions influenced by neutral particles is confirmed by figure 18. For ctr-injection, most charge exchange particles are in trapped orbits. With regard to co-injection, the majority of the charge exchange particles are in passing orbits. If not bounded by lost confined boundary, the charge exchange will increase the overall particle loss fraction. For ctr-tang, the charge exchange particles are bounded by lost confined boundary, which explains that the presence of neutral particles has a limited effect on the overall particle loss fraction of ctr-tang.

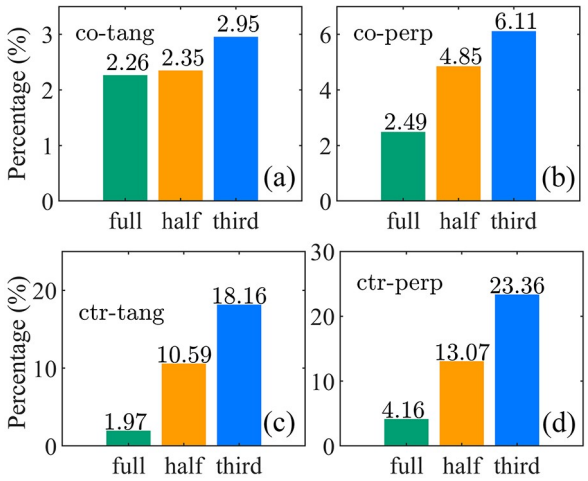

Figure 17. Ratios of charge exchange of three different energies of (a)–(d) four injections, which is defined as the ratio of the number of charge exchange particles to the number of injected particles. The green, orange, and blue columns correspond to particles with full energy, half energy, and one-third energy, respectively.

Table 3 gives the effect of neutral particles on loss fraction. In the presence of neutral particles, among the four injection configurations, the ctr-perp injection exhibits the most significant variation in particle loss fraction, ranging from 18.56% to 25.42%. From figure 19(g), it is evident that the presence of neutral particles has an almost negligible influence on lost ions in ctr-perp injection, as can be seen from the peak values (69.37 kW/m²) and the overall trends in the distribution of lost power density for ions remain consistent. This means in ctr-perp injection, the fast ions undergoing charge exchange are all confined particles, which can be validated from figure 18(d). From figure 19(h), it is evident that the peak value (1.67 kW/m²) of lost power density of neutrals is significantly lower than the peak value (69.37 kW/m²) of lost power density of ions. Unlike ions, whose loss power density is localized around $\Theta = 2\pi$, the lost power density distribution of neutral particles is random, which is correlated with charge exchange processes occurring at different phases during particle gyration. In ctr-perp injection, as discussed above, a substantial population of trapped particles exists on the low field side, their entire poloidal trajectories lie within the neutral-rich region, and most of the particles undergoing charge exchange are confined particles. These explain the significant effect of charge exchange on the particle loss fraction of the ctr-perp injection. In contrast to ctr-perp, the effect of charge exchange on particle loss fraction of ctr-tang is negligible, with the loss fraction ranging from 31.21% to 32.86%. Figure 19(e) illustrates that the presence of neutral particles reduces the peak value of lost power density of the ions from 55.88 kW/m² to 48.17 kW/m². This reduction means that the

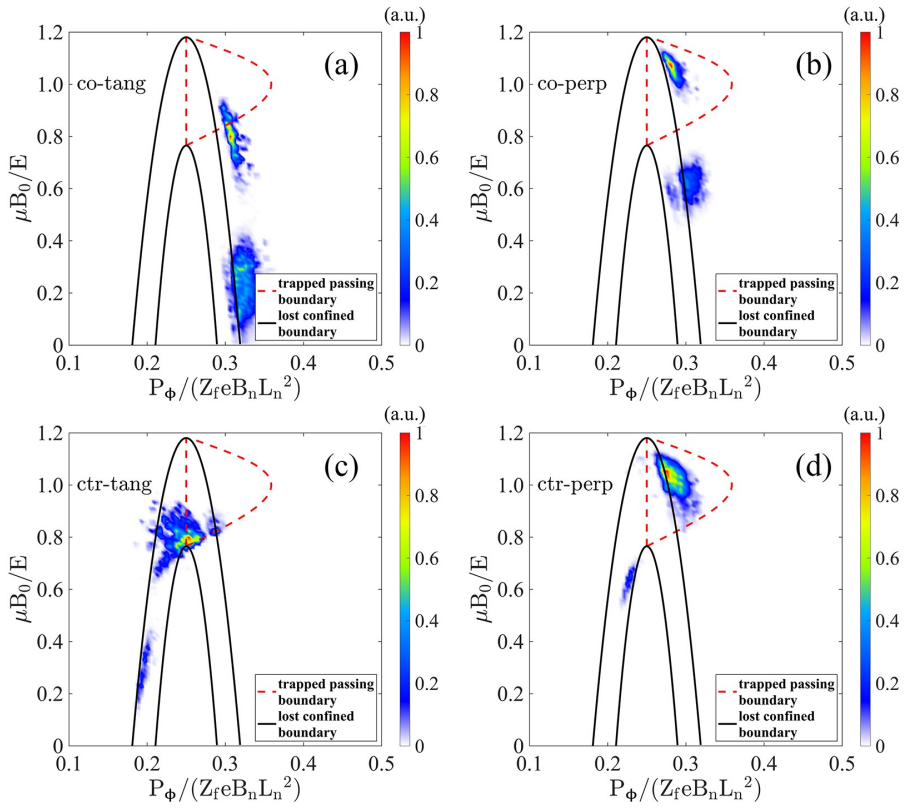

Figure 18. Distributions of charge exchange fast ions in (Λ, P_n) plane of (a)–(d) four injections.

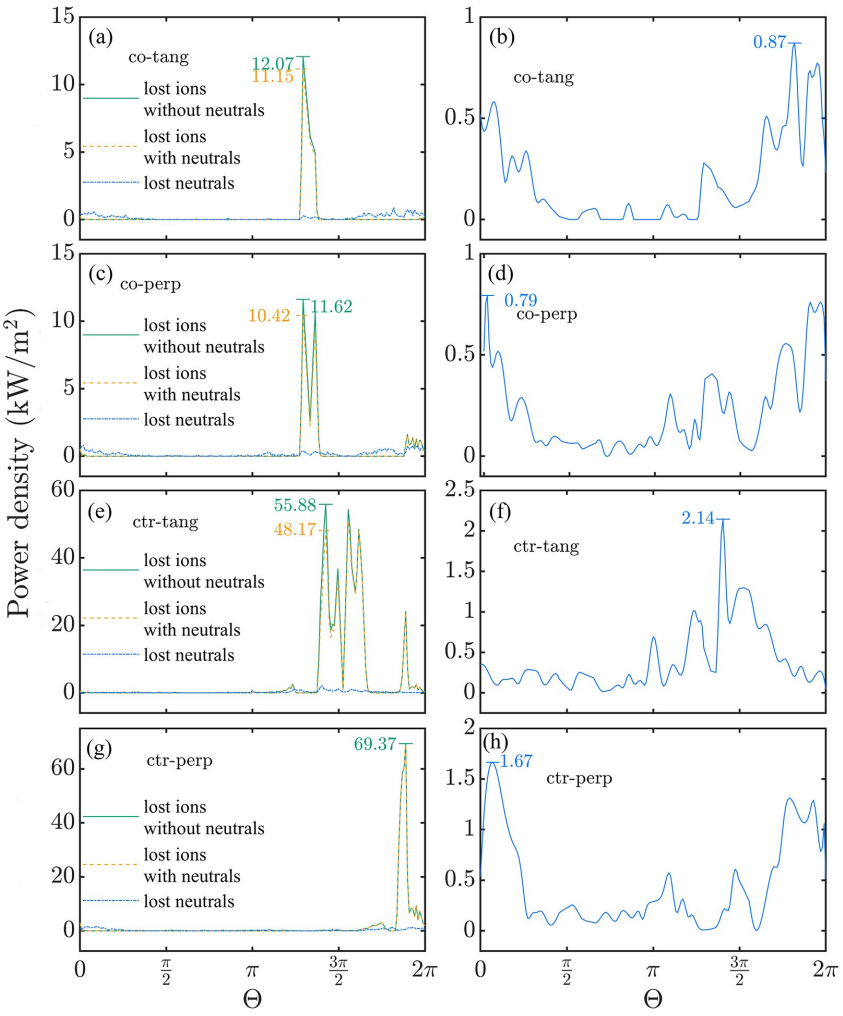

Figure 19. Effect of neutral particles on lost power density of (a)–(h) four injections. Left: the comparison of lost ions without neutrals, lost ions with neutrals and lost neutrals. Right: lost power density of neutrals from left figure with resized *y*-axis.

Table 3. The loss fraction of fast ions under the effect of neutrals.

Injection direction	Loss fraction (%)	
	Without neutrals	With neutrals
co-tang	1.38	3.60
co-perp	1.98	4.92
ctr-tang	31.21	32.86
ctr-perp	18.56	25.42

charge exchanges process of ctr-tang occurs primarily with ions that are on the verge of loss but have not yet undergone it. This is also confirmed by the fact that most of the charge exchange occurs near the lower divertor and the distribution of charge exchange ions in (Λ, P_n) plane is bounded by lost confined boundary, as shown in figures 14(c), 16(c) and 18(c). Therefore, the presence of neutral particles has a limited effect on the overall particle loss fraction of ctr-tang. This is because many ions which are about to lose can experience charge exchange and are subsequently lost in the form of neutral particles, resulting in a transformation of the loss process without a significant change in the total loss fraction.

In the case of co-tang injection, an effective confinement of fast ions is observed, with a particle loss fraction of 1.38% in the absence of neutral particles. However, the introduction of neutral particles leads to a notable increase in the total loss fraction by a factor of 2.6 compared to the value in the absence of neutral particles. It should be noted that while the loss fraction in the presence of neutral particles is not excessively high, there is still a noticeable increase. From figure 19(a), it can be seen that the peak value of lost power density of ions decreases from 12.07 kW/m² to 11.15 kW/m² due to the occurrence of charge exchange near the lower divertor. As shown in figure 19(b), the lost power density of neutral particles is mainly around the right side of the first wall and the lower left divertor. The peak value of lost power density of neutral particles, at 0.87 kW/m², is significantly lower than the corresponding value of ions, which is 11.15 kW/m². As for co-perp injection shown in figures 19(c) and (d), the effect of neutral particles is similar to that of co-tang injection, the only difference lies in the fact that, for co-perp injection, the neutral particles loss due to charge exchange exceeds that of co-tang injection. This difference can be attributed to the higher fraction of trapped particles associated with co-perp injection, which can be validated from figure 18(b).

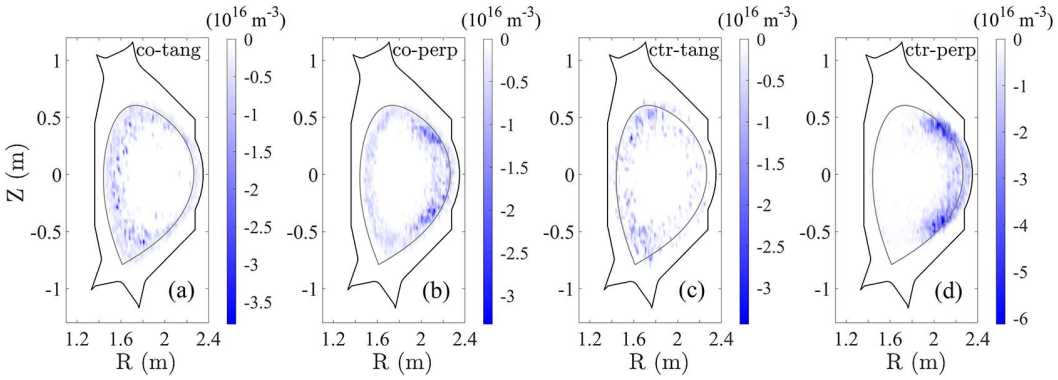

Figure 20. The difference between the fast ions density with neutral particles and the fast ions density without neutral particles of (a)–(d) four injections. Deeper shades of blue indicate a greater reduction in fast ion density.

Figure 20 illustrates the effect of charge exchange processes on the fast ion density of four injections. For tangential configurations, the reduction in fast ion density is primarily concentrated on the high field side. Conversely, for perpendicular configurations, a noticeable decrease in fast ion density is distributed over the low field side. For perpendicular configurations, the trapped particles on the low field side increase the possibility of charge exchange, hence, the reduction in fast ion density is primarily concentrated on the low field side. As for co-tang configuration, due to the gradient and curvature of the magnetic field, the poloidal trajectory of fast ion will drift towards high field side, resulting in the charge exchange on high field side. For ctr-tang configuration, a considerable fraction of fast ions deposited on the low field side are lost due to curvature and gradient drift effects, therefore, the fast ions whose depositions are deep into plasma have a higher possibility to experience charge exchange process. Hence, the reduction of fast ion density is primarily on the high field side. Furthermore, as shown in figure 20(d), the charge exchange effect is most pronounced for ctr-perp injection. In terms of the neutral particle loss fraction induced by charge exchange, ctr-injection exceeds co-injection, and perpendicular configuration exceeds tangential configuration. For co-injection, the cumulative neutral particles loss outweighs the total ions loss when neutral particles are absent at the edge. However, the peak value of the lost power density of neutral particles is significantly lower than the peak value of lost power density of ions.

Figure 21 depicts the effect of charge exchange on current drive. The impact on current drive primarily occurs near the edge (ρ= 0.7−0.9), corresponding to the charge exchange position. The influence of charge exchange on current, denoted by ΔI, is 0.829 kA/MW for the co-tangential and 0.451 kA/MW for the co-perpendicular configurations. When compared to the NBI current drive efficiency of 25 kA/MW in EAST, the effect of charge exchange on current drive appears relatively moderate.

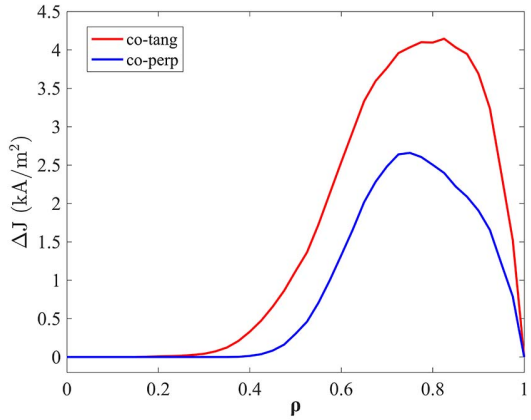

Figure 21. Radial profiles of current drive influenced by charge-exchange, ρ is the normalized radius and ΔJ is the difference of current density between the case without charge-exchange and with charge-exchange.

3.3. Losses with neutrals and reionization

When taking reionization into account, particles that undergo charge exchange may enter the bulk plasma as neutrals and subsequently experience reionization in the core, often following better confined orbits. The loss fractions of neutrals and reionization ions of four injections are shown in figure 22, where the blue and orange bars correspondingly depict the loss fractions of neutral particles and reionization ions. In figure 22, column “a” and column “b” denote the loss fraction considering reionization and the loss fraction excluding reionization, respectively. The difference in the blue segments between columns “a” and “b” represents the

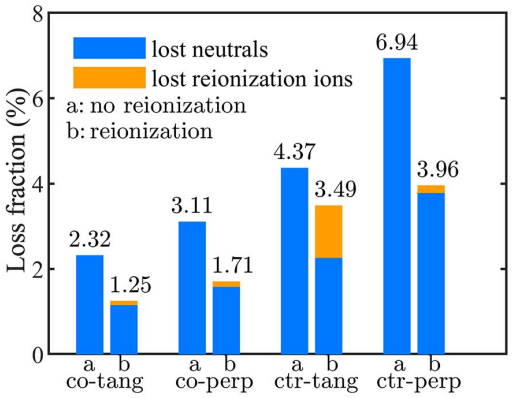

Figure 22. Lost fractions of neutrals and reionization ions when reionization is considered.

effect of reionization on the loss of neutral particle, the greater difference indicates the higher occurrence of particles undergoing reionization. It is evident that reionization leads to a reduction of approximately 50% in the fraction of lost neutral particles of four injections, which is due to the gyro motion of fast ions before undergoing charge exchange. The orange segment in column "b" symbolizes the lost reionization ions, with a larger segment indicating more loss. With the exception of ctr-tang injection, the reionization ions from the other three injections are well confined. From the distribution of the number of reionization particles shown in figure 23 and the poloidal distribution of density of reionization particles shown in figure 24, it is found that for ctr-tang injection, the reionization process occurs primarily near the lower side of the divertor, while for the other three injections, the reionization process takes place mainly on the low field side.

Figure 25 illustrates the effects of charge exchange processes and reionization processes on the fast ion density of four injections. For perpendicular injection, the loss of fast ion density is primarily concentrated on the low field side of the LCFS, whereas for tangential injection, the loss of fast ion density is mainly concentrated on the high field side of the LCFS. This phenomenon is consistent with the results of figure 20. Furthermore, the increase of fast ion density in the core region of perp-injection exceeds that of tangential injection. The loss fraction and density distribution of fast ions of ctr-perp injection are most influenced by the effects of charge exchange and reionization among four injections. The influence of charge exchange and reionization on heating power density of ctr-perp injection is shown in figure 26. The power affected by charge exchange primarily concentrates on the low-field side, accompanied by a small amount of power loss on the high-field side. The heat-

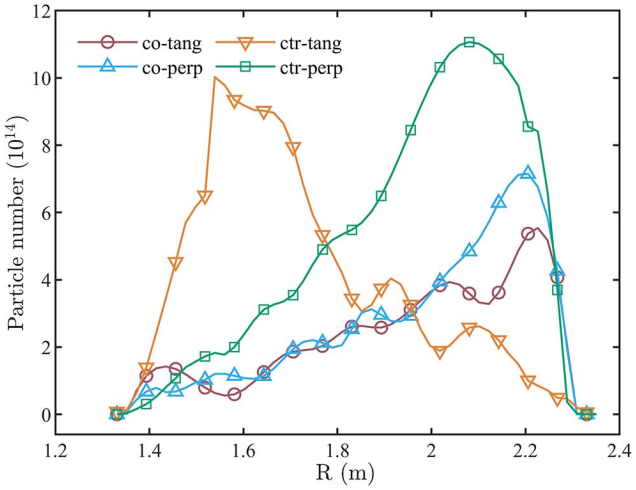

Figure 23. Distributions of reionization particles number of four injections.

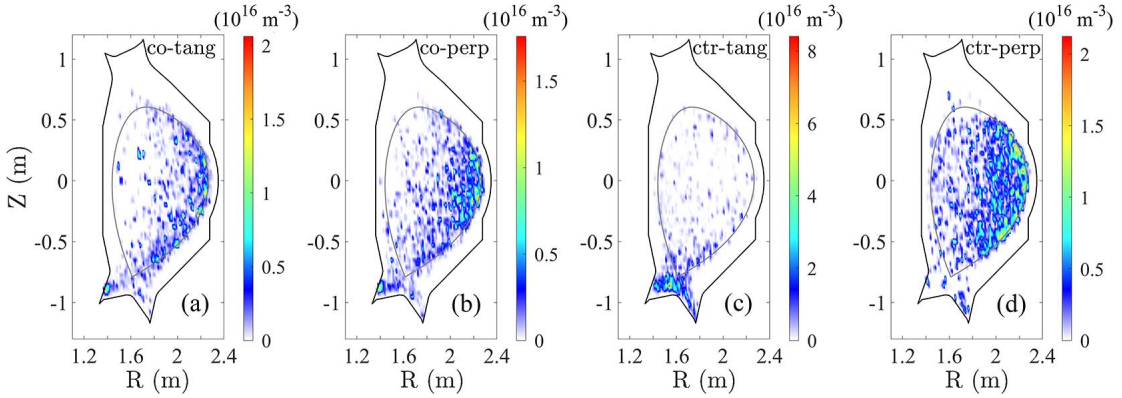

Figure 24. Poloidal distributions of density of reionization particles of (a)–(d) four injections.

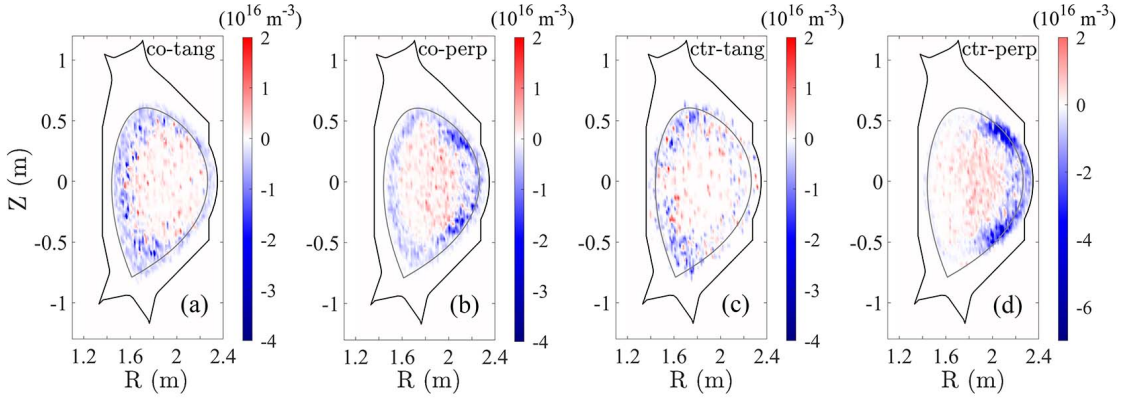

Figure 25. The difference between the fast ion density with the effects of neutral particles (including charge exchange and reionization) and the fast ions density without the effects of neutral particles of (a)–(d) four injections. Deeper shades of blue and red correspond to more decrease and increase in fast ion density, respectively.

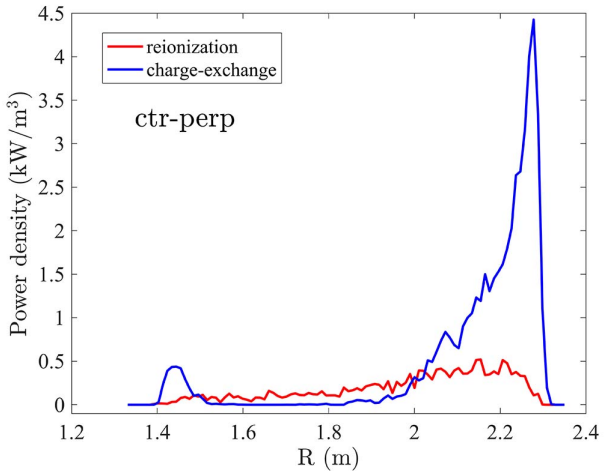

Figure 26. Heating power density influenced by charge-exchange and reionization. The blue line indicates the power density taken away by charge-exchange and the red line shows the power density given back by reionization.

ing power taken away by charge exchange is approximately 0.06 MW.

4. Discussion and conclusion

In this article, we have employed the test particle code PTC to perform numerical simulations to investigate the influence of neutral particles in the edge on fast ions originating from the NBI on EAST device. Owing to charge exchange reaction, fast ions born near the edge or travelling to the edge have the potential to transform into fast neutrals, contributing to an elevated heat load on the first wall. When considering re-ionization process, about half of these fast neutrals will directly lose to the first wall, while the rest will re-enter the plasma and ionize again, bringing energy to bulk plasma.

In the simulation presented in this article, four beam sources were considered: co-tang, co-perp, ctr-tang and ctr-perp. When considering the influence of neutral particles, the ctr-perp injection demonstrates the most significant variation in particle loss fraction among the four injection configurations, while the influence of charge exchange on the particle loss fraction of ctr-tang is found to be negligible. This can be attributed to the fact that the fast ions of ctr-perp undergoing charge exchange are all confined trapped particles, whereas the fast ions of ctr-tang undergoing charge exchange are on the verge of loss. For co-injection, with the effective confinement, the loss fraction of fast ions is not excessively high, but the increase of the loss fraction in the presence of neutral particles is evident. Compared to the localized heat load in the absence of neutral particles, the heat load due to charge exchange exhibits randomness correlated with charge exchange processes occurring at different phases during particle gyration. With respect to the loss fraction of neutral particle resulting from charge exchange, ctr-injection exceeds co-injection and the perpendicular configuration demonstrates a higher fraction compared to the tangential configuration. The difference of charge exchange ratios of three different energies of the four injections can be attributed to variations in the poloidal trajectories associated with each of these injections. When considering the influence of re-ionization, it is noteworthy that, with the exception of the ctr-tang injection, the reionized ions from the other three injections are confined well.

In the experiment, the neutral density near the edge remains insufficiently characterized. In EAST, the neutral density at some specific regions can be deduced indirectly from the D_α/H_α line emission intensity measured by photodiode array (PDA) system [17, 36], and the measuring result validates the accuracy of the neutral density calculated by the SOLPS-ITER to some extent. Furthermore, a diagnostic technique named imaging neutral particle analyzer (INPA) [37–41] has been installed in EAST to measure the density of neutral particles resulting from charge exchange reactions. INPA will be leveraged to experimentally detect charge exchange processes in different discharges. Additionally, due to the high first-orbit losses of ctr-injection, the beam lines originally situated in F-port will be moved to D-port and the ctr-injection will no longer exist [42]. Therefore, the influence of charge exchange on the fast ions from beam lines in D-port should be studied in future work. Moreover, the Toroidal Field Ripple (TFR) has not been considered in this simulation. The influence of the TFR on the trapped particles induces radial excursions, consequently increasing the possibility of experiencing charge exchange. We will consider the influence of TFR in the future. Besides, different plasma density will change the deposition of fast ions, thereby influencing the charge exchange. The simulations introduced in this paper do not extend to the discussion about the effects of plasma density. This will be the topic of future research.

Acknowledgments

This work was supported by the National Key R&D Program of China (No. 2022YFE03090000) and National Natural Science Foundation of China (No. 11975068).

References

[1] Scoville J T *et al* 2019 *Fusion Eng. Des.* **146** 6
[2] Heidbrink W W *et al* 2009 *Plasma Phys. Control. Fusion* **51** 125001
[3] Asunta O *et al* 2015 *Comput. Phys. Commun.* **188** 33
[4] Meade D M and The TFTR Team 1994 *J. Fusion Energy* **13** 145
[5] Budny R V *et al* 1995 *Nucl. Fusion* **35** 1497
[6] Jacquinot J and JET Team 1998 *Nucl. Fusion* **38** 1263
[7] Budny R V *et al* 2016 *Nucl. Fusion* **56** 056002
[8] Wesson J 2011 *Tokamaks* 4th ed (Oxford: Oxford Science Publications)
[9] Hu C D *et al* 2015 *Plasma Sci. Technol.* **17** 817
[10] Zhu Y B, Heidbrink W W and Pickering L D 2010 *Nucl. Fusion* **50** 084024

[11] Pace D C *et al* 2016 *Fusion Eng. Des.* **112** 14
[12] Zhao R *et al* 2020 *Plasma Phys. Control. Fusion* **62** 115001
[13] Xu X Y *et al* 2020 *Plasma Sci. Technol.* **22** 085101
[14] Wu B *et al* 2017 *Plasma Phys. Control. Fusion* **59** 025004
[15] He K *et al* 2021 *Nucl. Fusion* **61** 016009
[16] Hao B L *et al* 2019 *Nucl. Fusion* **59** 076040
[17] Zhang L *et al* 2011 *Plasma Sci. Technol.* **13** 431
[18] Zhang D R *et al* 2020 *Nucl. Fusion* **60** 106015
[19] Geiger B *et al* 2017 *Plasma Phys. Control. Fusion* **59** 115002
[20] Kramer G J, Van Zeeland M A and Bortolon A 2020 *Nucl. Fusion* **60** 086016
[21] Jaulmes F *et al* 2021 *Nucl. Fusion* **61** 046012
[22] Bonnin X *et al* 2016 *Plasma Fusion Res.* **11** 1403102
[23] Zhang C *et al* 2022 *Nucl. Fusion* **62** 076012
[24] Wang F *et al* 2021 *Chin. Phys. Lett.* **38** 055201
[25] Liu S J *et al* 2022 *J. Plasms Phys.* **88** 905880505
[26] Wu X F *et al* 2023 *Acta Phys. Sin*. **72** 181 (in Chinese)
[27] Pankin A *et al* 2004 *Comput. Phys. Commun.* **159** 157
[28] Schneider M *et al* 2011 *Nucl. Fusion* **51** 063019
[29] Wan B N *et al* 2017 *Nucl. Fusion* **57** 102019
[30] Wan B N *et al* 2019 *Nucl. Fusion* **59** 112003
[31] White R B and Chance M S 1984 *Phys. Fluids* **27** 2455
[32] White R B 1990 *Phys. Fluids B: Plasma Phys.* **2** 845
[33] Feng Y, Wolle B and Hübner K 1995 *Comput. Phys. Commun*. **88** 161Janev R K 1989, Nucl. Fusion, **29** 006
[34] Janev R K 1989 *Nucl. Fusion* **29** 2125
[35] Janev R K *et al* 1987 *Elementary Processes in Hydrogen-Helium Plasmas* (Berlin: Springer)
[36] Zhang P F *et al* 2018 *Plasma Sci. Technol.* **20** 045104
[37] the W7X-Team 2022 *J. Instrum.* **17** P01034
[38] Lin D J *et al* 2020 *Nucl. Fusion* **60** 112008
[39] Civinini C *et al* 2017 *J. Instrum.* **12** C01034
[40] Schneider P A *et al* 2015 *Rev. Sci. Instrum.* **86** 073508
[41] Jacobsen A S *et al* 2016 *Plasma Phys. Control. Fusion* **58** 045016
[42] Xie Y H *et al* 2022 *IEEE Trans. Plasma Sci.* **50** 4086
[43] Burrell K H *et al* 2002 *Plasma Phys. Control. Fusion* **44** A253
[44] Helander P, Akers R J and Eriksson L G 2005 *Phys. Plasmas* **12** 112503
[45] Liu H Q *et al* 2014 *Rev. Sci. Instrum.* **85** 11D405
[46] Zang Q *et al* 2016 *Nucl. Fusion* **56** 106003
[47] Li Y Y *et al* 2014 *Rev. Sci. Instrum.* **85** 11E428